

The ambiguity of context-specific metabolic model predictions

Semidán Robaina-Estévez, Zoran Nikoloski

Systems Biology and Mathematical Modeling Group, Max Planck Institute of Molecular Plant Physiology, Potsdam-Golm, Germany

Abstract

The integration of experimental data into genome-scale metabolic models can greatly improve flux predictions. This is achieved by restricting predictions to a more realistic context-specific domain, like a particular cell or tissue type. Several computational approaches to integrate data have been proposed — generally obtaining context-specific (sub)models or flux distributions. However, these approaches may lead to a multitude of equally valid but potentially different models or flux distributions, due to possible alternative optima in the underlying optimization problems. Although this issue introduces ambiguity in context-specific predictions, it has not been generally recognized, especially in the case of model reconstructions. In this study, we analyze the impact of alternative optima in four state-of-the-art context-specific data integration approaches, providing both flux distributions and/or metabolic models. To this end, we present three computational methods and apply them to two particular case studies: leaf-specific predictions from the integration of gene expression data in a metabolic model of *Arabidopsis thaliana*, and liver-specific reconstructions derived from a human model with various experimental data sources. The application of these methods allows us to obtain the following results: (i) we sample the space of alternative flux distributions in the leaf-specific case and quantify the ambiguity of the predictions. In addition, we show how the inclusion of ℓ_1 -regularization during data integration reduces the ambiguity in this case. (ii) We generate sets of alternative leaf- and liver-specific models that are optimal to each one of the evaluated model reconstruction approaches. We demonstrate that alternative models of the same context contain a marked fraction of disparate reactions. Further, we show that a careful balance between model sparsity and metabolic functionality helps in reducing the discrepancies between alternative models. Finally, our findings indicate that alternative optima must be taken into account for rendering the context-specific metabolic model predictions less ambiguous.

Author Summary

Recent methodological developments have facilitated the integration of high-throughput data to obtain context-specific metabolic reconstructions. A unique solution to this data integration problem often may not be guaranteed, leading to a multitude of context-specific predictions equally concordant with the integrated data. Yet, little attention has been paid to the alternative optima resulting from the integration of context-specific data. Here we present computational approaches to analyze alternative optima for different context-specific data integration instances. By using these approaches on metabolic reconstructions for the leaf of *Arabidopsis thaliana* and the human liver, we show that the analysis of alternative optima is key to adequately evaluating the specificity of the predictions in particular cellular contexts. While we provide several ways to reduce the ambiguity in the context-specific predictions, our findings

indicate that the existence of alternative optimal solutions warrant caution in detailed context-specific analyses of metabolism.

Introduction

Genome-scale metabolic models (GEMs) have proven instrumental in characterizing the activity of metabolic pathways in different biological scenarios. The activity of all metabolic reactions is specified by the flux distribution, which can be readily inferred from GEMs through the usage of constraint-based approaches (1,2). Such approaches often infer fluxes as solutions to a convex optimization problem in which an objective function is optimized under specified constraints. Two types of constraints can generally be considered: The first is due to the stoichiometry, thermodynamic viability and mass-balance conditions. These constraints are included in every constraint-based approach. The second type comprises constraints specific to each approach, and usually reflects the context-specific knowledge or data to be integrated. Flux distributions which satisfy the set of constraints are called feasible. A convex optimization problem is guaranteed to render a unique optimal value (3). However, it is not always guaranteed that there is a unique flux distribution realizing the optimal objective value, leading to alternative optimal flux distributions. Indeed, such a space of alternative optima arises even in the case of flux balance analysis (FBA), as a classical representative of constraint-based approaches (4–9).

Experimental systems biology studies have generated comprehensive atlases of transcript, protein, and metabolite levels from different context, such as: cell types, developmental stages, and environments, across different species from all kingdoms of life (10–15). Analyses of these data sets have already pointed that context-specific differences in the levels of molecular components often affect the activity of metabolic pathways. Additionally GEMs allow constraint-based approaches to integrate such data sets through the so-called gene-protein-reaction rules, which relate metabolic reactions with the enzymes involved and their coding genes. These approaches address two aims: (i) obtaining context-specific flux distribution and (ii) determining context-specific GEMs; we refer to the respective approaches as flux- and network-centered, respectively. However, here too, alternative optima may also result from the integration of context-specific data. Yet, only two flux-centered approaches, iMAT (16) and InDisMinimizer (17), recognized this issue and proposed a way to investigate the space of alternative optima. Moreover, studies focusing on network-centered approaches did not acknowledge the possibility of alternative optimal context-specific networks. In both settings, the existence of alternative optima leads to ambiguity in context-specific flux distributions and/or network reconstructions, since alternative solutions may substantially differ. This is particularly important in the case of context-specific network reconstructions, where further investigations conducted on a single optimal network could lead to erroneous conclusions. In the present study, we analyze alternative optimal solutions resulting from context-specific data integration in flux-centered and network-centered approaches.

This study is organized in two parts. The first part is devoted to explain the mathematical and computational logic of both (i) the context-specific data integration approaches herein evaluated, and (ii) the methods that we propose to analyze their alternative optima. The second part presents the findings obtained from applying the previously described methods to two particular case studies: a leaf-specific reconstruction from the model plant *Arabidopsis thaliana*, and a human liver reconstruction. This second part serves as an illustration of the impact that alternative optima have in context-specific metabolic reconstructions, and may be followed independently from the first part — which is primarily addressed to the specialized reader.

Results and discussion

Evaluation of alternative optima from context-specific data integration approaches: Computational methods

In this section, we present the mathematical formulation of the computational methods that we developed to investigate the alternative optima of three selected data integration approaches. In all three cases, we first provide an overview of the approach, which is followed by a description of the method to explore its alternative optima space. We start by a representative of a flux-centered approach — a modified version of RegrEx (18) — and the method that we propose to explore its alternative optima, termed RegrEx Alternative Optima Sampling (RegrEx_{AOS}). We then focus on Core Expansion (CorEx), also developed in this study, which we take as representative of a network-centered approach. In addition, we show how the optimization program behind CorEx can be adapted to evaluate not only its alternative optima space, but that of FastCORE (19) and CORDA (20), two state-of-the-art network-centered approaches. We conclude the section with the iMAT approach, since it ranks among the very few for which a means to investigate its alternative optima was proposed in the original publication (16). Here we revisit the original method, and propose a complementary way to investigate its alternative optima space.

Alternative optima in flux-centered approaches: the case of RegrEx

Background

Given a GEM and (context-specific) gene or protein expression data, the Regularized metabolic model Extraction (RegrEx) method reconstructs a context-specific metabolic model, along with the corresponding flux distribution. To this end, RegrEx finds a feasible flux distribution that is closest to a given experimental data set, and is, therefore, considered a flux-centered approach.

The original RegrEx approach relied on a regularized least squares optimization in which the Euclidean distance between the given gene expression data vector, d , and a feasible flux distribution, v , *i.e.*, the squared ℓ_2 norm of the difference vector $\epsilon = d - v$, was minimized (18). The regularization was implemented by also considering the (weighted) ℓ_1 norm of v in the minimization problem, as a means to select the reactions in the GEM that are most important for a given metabolic context. However, here we used a slightly modified version of RegrEx: Instead of minimizing the sum of square errors, we minimize the sum of absolute errors, *i.e.*, the ℓ_1 norm of ϵ . Except for this substitution, the modified RegrEx version, called RegrEx_{LAD} (for Least Absolute Deviations), follows the same formulation as the original RegrEx (see S1 Appendix for detailed comparison).

The minimization problem behind RegrEx_{LAD} considers a set of constraints required to handle reversible reactions: In this case, absolute flux values must be taken into account when minimizing the distance to the (non-negative) associated gene expression (*i.e.*, for a reversible reaction i , $\epsilon_i = |v_i| - d_i$). This is accomplished through splitting reversible reactions into the forward and backward directions, each constrained to have non-negative flux value, and introducing a vector of binary variables, x , to select only one of them during the optimization. Altogether, these particularities are captured in the mixed integer linear program (MILP),

$$\begin{aligned}
v_{opt} &= \arg \min_w^T (\epsilon^+ + \epsilon^-) + \lambda \|v\|_1 \\
\epsilon^+ &= [\epsilon_{irr}^+, \epsilon_{for}^+, \epsilon_{back}^+], \\
\epsilon^- &= [\epsilon_{irr}^-, \epsilon_{for}^-, \epsilon_{back}^-], \\
v &= [v_{irr}, v_{for}, v_{back}] \in \mathbb{R}_0^+, \\
x &\in \{0,1\}^n \\
s.t. \\
1. \quad S_{ext} v &= 0 \\
2. \quad v_{irr_i} + (\epsilon_{irr}^+ - \epsilon_{irr}^-) &= d_{irr} \\
3. \quad v_{for_i} + (\epsilon_{for}^+ - \epsilon_{for}^-) + x d_{revRxn_s} &= d_{revRxn} \\
4. \quad v_{rev_i} + (\epsilon_{back}^+ - \epsilon_{back}^-) - x d_{revRxn} &= 0 \\
5. \quad v_{irr_{min}} \leq v_{irr} \leq v_{irr_{max}} \\
6. \quad v_{for} + x v_{for_{min}} &\geq v_{for_{min}} \\
7. \quad v_{back} - x v_{rev_{min}} &\geq 0 \\
8. \quad v_{for} + x v_{for_{max}} &\leq v_{for_{max}} \\
9. \quad v_{back} - x v_{rev_{max}} &\leq 0
\end{aligned} \quad \left. \vphantom{\begin{aligned} 2. \\ 3. \\ 4. \end{aligned}} \right\} i \in Data - bounded \quad (OP_1).$$

In OP_1 , the flux distribution, v , is partitioned into the sets of irreversible (v_{irr}), and reversible reactions proceeding into the forward (v_{for}) and backward directions (v_{back}), and the (reaction) columns of the stoichiometric matrix, S_{ext} , are ordered to match the partition of v . In addition, the components of the error vector, $\epsilon_i = \epsilon_i^+ - \epsilon_i^-$, $\epsilon_i^+, \epsilon_i^- \geq 0$, are split into two non-negative variables, $\epsilon_i^+, \epsilon_i^-$, as a way to computationally treat the otherwise required absolute values of the components of ϵ . Thus, the ℓ_1 norm $\|\epsilon\|_1 = \sum_i |\epsilon_i|$ is replaced by $\epsilon_i^+ + \epsilon_i^-$ in the objective function. Finally, the λ parameter corresponds to the weight of the ℓ_1 norm in the objective function, and is chosen during the optimization as to maximize the Pearson correlation between data and flux values (18).

The convexity of OP_1 guarantees finding the minimum distance between experimental data and a feasible flux distribution that is allowed by the constraints. However, it does not guarantee that the resulting flux distribution is the only feasible one that is optimal with respect to a particular context-specific data. This variability in optimal flux distributions may be attributed to two factors. On the one hand, as mentioned above, not all reactions in a GEM are typically associated to data. In contrast to *data-bounded* reactions, there is a set of *data-orphan* reactions comprising non-enzymatically catalyzed reactions, reactions without gene-protein annotation or without associated data for a particular context. Data-orphan reactions do not contribute to the error norm in the RegrEx_{LAD} objective function, described in OP_1 , and their flux value can vary as long as v satisfies the imposed constraints and its ℓ_1 norm is preserved. This situation is depicted in Fig 1, where the search for a flux distribution v that is closest to the data vector, d , is carried out in the projection of the flux cone, $F = \{v: Sv = 0, v_{min} \leq v \leq v_{max}\}$, where d resides. On the other hand, the geometry of F may preclude certain reactions to obtain an exact match with the data value, when d remains outside the projection of F . In this case, a set of flux distributions may be equidistant to d , thus generating variability also in the optimal flux value of data-bounded reactions.

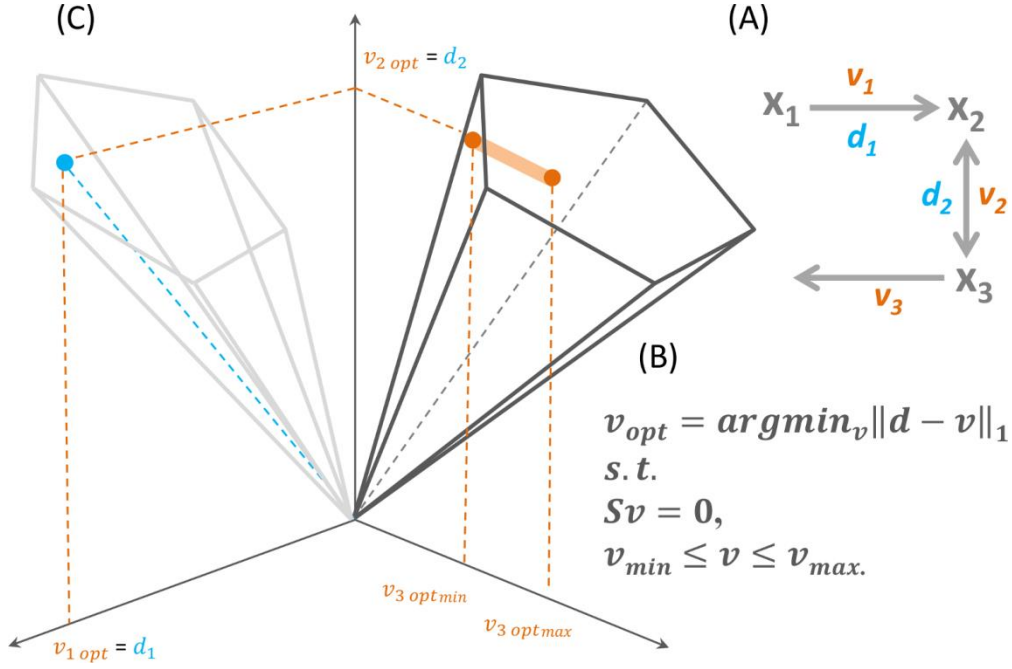


Fig 1. A depiction of the alternative optima space of a toy RegrEx data integration problem. (A) A toy data integration problem for a metabolic network with three reactions, v_{1-3} , and two reaction-associated data values, d_{1-2} is presented. In RegrEx, the optimization problem consists of finding a flux distribution, v_{opt} , which minimizes the distance to the data being integrated and is compatible with the mass balance and thermodynamic constraints. In this example, only two of the three reactions are data-bounded; thus, the third, v_3 , is free to vary its flux value without affecting the minimum overall distance in (B). This situation is depicted in (C), where the flux cone (the set of flux distributions, v , that are compatible with the imposed constraints) is projected onto the two-dimensional space where the data vector, d , resides, and the search for the optimal, v_{opt} is conducted on this projection. This implies that v_3 can vary along the direction orthogonal to the projection plane, as long as its value remains within the flux cone (here depicted as the orange line crossing the cone). Hence, the alternative optima space of this data integration problem consists of alternative vectors, $v_{opt(i)}$, in which the components v_1 and v_2 are fixed, and v_3 varies between $v_{3optmin}$ and $v_{3optmax}$.

The RegrEx alternative optima sampling method

The general approach followed by RegrEx_{AOS}, depicted in Fig 2, is similar to the Flux Variability Sampling (17) (here adapted to RegrEx_{LAD}, see S1 Appendix). RegrEx_{AOS} first creates a random flux vector, v_{rand} , which is bounded by the maximum and minimum flux values previously calculated by Flux Variability Analysis (using only upper and lower bounds as constraints, see Methods). It then searches for the closest flux vector, v , to v_{rand} that belongs to the alternative optima space, *i.e.*, it is at the same distance to the data vector, d , and has the same ℓ_1 norm as the previously calculated RegrEx_{LAD} optimum. This is performed by solving the MILP given in OP₂. Finally, RegrEx_{AOS} iterates this routine n times to obtain a sufficiently large sample; here we used $n = 2000$.

$$\begin{aligned}
& \min \quad \|\delta^+ + \delta^- + \delta_{back}\|_1 \\
& \epsilon^+ = [\epsilon_{irr}^+, \epsilon_{for}^+, \epsilon_{back}^+], \\
& \epsilon^- = [\epsilon_{irr}^-, \epsilon_{for}^-, \epsilon_{back}^-], \\
& \delta^+ = [\delta_{irr}^+, \delta_{for}^+], \\
& \delta^- = [\delta_{irr}^-, \delta_{for}^-], \\
& v = [v_{irr}, v_{for}, v_{back}] \in \mathbb{R}^+, \\
& x \in \{0, 1\}^n \\
& s.t. \\
& 1 - 9 \quad (\text{OP}_1) \\
& 10. \quad \epsilon^+ + \epsilon^- = \epsilon_{opt}^+ + \epsilon_{opt}^- \\
& 11. \quad \|v\|_1 = \|v_{opt}\|_1 \\
& 12. \quad v_{irr} - (\delta_{irr}^+ - \delta_{irr}^-) = v_{rand(irr)} \\
& 13. \quad v_{for} - (\delta_{for}^+ - \delta_{for}^-) - xv_{rand(revRxn)} = 0 \\
& 14. \quad -v_{back} + \delta_{back} + xv_{rand(revRxn)} = v_{rand(revRxn)}
\end{aligned} \tag{OP}_2.$$

OP₂ inherits constraints 1-9 from OP₁ and incorporates two sets of new constraints. Constraints 10 and 11 are added to guarantee that v renders the same similarity to data and the same ℓ_1 norm of the previously found RegrEx_{LAD} optimum, v_{opt} , respectively. In addition, constraints 12-14 introduce the auxiliary variables δ_{irr} , δ_{for} and δ_{back} quantifying the distance of an optimal flux distribution to the randomly generated v_{rand} . More specifically, $\delta_{irr(i)} = \delta_{irr(i)}^+ - \delta_{irr(i)}^- = v_{rand(i)} - v_{irr(i)}$, $i \in I_R$, acts over the set of irreversible reactions (I_R) and $\delta_{for(i)} = \delta_{for(i)}^+ - \delta_{for(i)}^- = v_{rand(i)} - v_{for(i)}$, $\delta_{back(i)} = v_{rand(i)} - v_{back(i)}$, $i \in R_R$, over the set of reversible reactions (R_R). Note that both δ_{irr} , δ_{for} , are defined as the difference of two non-negative components, which enables us to formulate a linear objective function that renders OP₂ computationally tractable. In contrast, δ_{back} does not require this treatment since it always takes non-negative values (see Fig 2). This is because in OP₂, the stoichiometric matrix, S , corresponding to the GEM is first modified in the following way: we change the sign of the columns, as well as the entry in v_{rand} , corresponding to reversible reactions that were randomly assigned a negative flux value in v_{rand} . In this manner, all reversible reactions in v_{rand} operate in forward direction (*i.e.*, are non-negative) which facilitates the optimization process. In addition, δ_{for} and δ_{back} are constrained to be mutually exclusive by the same binary variable, x , introduced to select only one of the directions in reversible reactions (*i.e.* either forward or backward). In this manner, OP₂ will select the direction of reversible reactions that minimizes the overall distance to v_{rand} . Finally, reversible reactions whose sign was originally changed in v_{rand} are altered back to their original directions and their sampled flux values are modified accordingly.

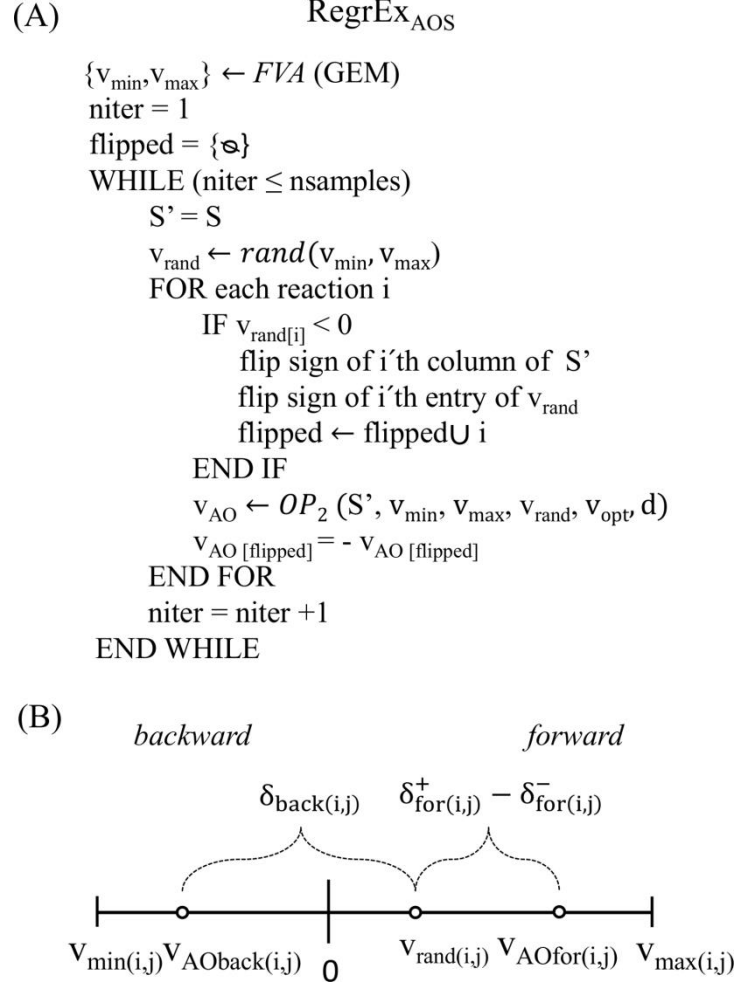


Fig 2. Pseudocode followed by $\text{RegrEx}_{\text{AOS}}$ and detail of the treatment of reversible reactions. (A) $\text{RegrEx}_{\text{AOS}}$ first finds the minimum, v_{\min} , and maximum, v_{\max} , allowable flux values through Flux Variability Analysis (FVA, see Methods) for each reaction in the GEM. It then repeats the following procedure until obtaining the required number of samples (nsamples). (i) Generate a random flux distribution, v_{rand} , in which each random flux value remains within the feasible range obtained before. (ii) Change the sign of the negative entries in v_{rand} and of the corresponding columns in the stoichiometric matrix. (iii) Generate an alternative optimal flux distribution, v_{AO} , that is closest to v_{rand} through OP_2 , which takes the modified stoichiometric matrix, S' , v_{\min} , v_{\max} , v_{rand} , the previous optimum RegrEx solution, v_{opt} and the data vector, d , as arguments. (iv) Change the sign of the entries in v_{AO} corresponding to the original negative entries in v_{rand} . (B) In $\text{RegrEx}_{\text{AOS}}$, reversible reactions are split into the forward and backward directions. The entries corresponding to reversible reactions in v_{rand} are always non-negative (since the sign is changed if negative), and fall in the range of the corresponding forward direction (since the sign of the associated column in S is changed accordingly). Hence $\text{RegrEx}_{\text{AOS}}$ can choose between $\delta_{\text{for}^+} - \delta_{\text{for}^-}$, quantifying the distance between v_{rand} and an optimal flux value in the forward direction, or δ_{back} , which measures the distance between v_{rand} and an optimal flux value in the backward direction. At the end of the optimization process (OP_2), $\text{RegrEx}_{\text{AOS}}$ selects the direction of each reversible reaction that minimizes the overall distance to v_{rand} .

Alternative optimal solutions in network-centered approaches: the case of CorEx

In this section, we analyze the alternative optimal solutions of CorEx, a method that we developed in this study to represent the network-centered approaches. In a general sense,

network-centered approaches first partition the set $R = C \cup P$ of reactions in the original GEM into a core set, C , that must be present in the final context-specific model, and a non-core set, P , which does not necessarily have to be in the final model. These approaches find then a subset $P_A \subseteq P$ of non-core reactions that renders C consistent, *i.e.*, all reactions in the core are able to carry a non-zero flux in at least one steady-state solution. The final context-specific subnetwork is then defined as $R_A = C \cup P_A$. Some approaches, like MBA (21), mCADRE (22) and FastCORE (19), aim at minimizing the size of P_A , as to obtain a parsimonious final model. In contrast, CORDA (20) relaxes the parsimony condition as a way to prevent eliminating important reactions for a given context. In this respect, CorEx aims at obtaining a parsimonious model, although, as shown in the following, it can be easily adapted to allow increasing the size of P_A if desired.

CorEx follows the MILP displayed in OP₃, which minimizes the number of reactions with non-zero flux in P while constraining all reactions in the core to carry at least a small positive flux (ϵ in constraints 2-3). This is achieved by minimizing the norm of the vector, x , of binary variables (constraints 4-7) which selects the set P_A that renders the MILP feasible. Note that the selected non-core reactions are forced to carry a small positive flux (constraints 5, 7) to guarantee that they are active in the final context-specific model. Finally, like in RegrEx, reversible reactions are split into the forward and backward directions, to operate only with non-negative flux values. In addition, another set of binary variables, y in constraints 8-9 of OP₃, is introduced to select the direction of reversible reactions (*i.e.*, imposing $v_{for} > XOR \ v_{back} > 0$, when the reaction is selected to be active).

$$\begin{aligned}
Z &= \min \quad ||x||_1 \\
v &= [v_{irr}, v_{for}, v_{back}] \in \mathbb{R}^{r+}_0, \\
x &= [x_{irr}, x_{rev}] \in \{0,1\}^p \\
y &\in \{0,1\}^{rev} \\
s.t. \\
1. \quad S_{ext} v &= 0 \\
2. \quad v_{irr(i)} &\geq \epsilon \\
3. \quad v_{for(i)} + v_{back(i)} &\geq \epsilon \\
4. \quad v_{irr(i)} - x_{irr(i)} v_{max} &\leq 0 \\
5. \quad v_{irr(i)} - x_{irr(i)} \epsilon &\geq 0 \\
6. \quad (v_{for(i)} + v_{back(i)}) - x_{rev(i)} v_{max} &\leq 0 \\
7. \quad (v_{for(i)} + v_{back(i)}) - x_{rev(i)} \epsilon &\geq 0 \\
8. \quad v_{for} + y v_{max} &\leq v_{max} \\
9. \quad v_{back} - y v_{max} &\leq 0
\end{aligned} \quad \left. \begin{array}{l} \\ \\ \\ \end{array} \right\} \quad , \quad i \in C \quad (OP_3).$$

To identify alternative optimal CorEx extracted networks, we developed the MILP displayed in OP₄. The general idea behind OP₄ is to find the most dissimilar context-specific network, $R_{A^*} = C \cup P_{A^*}$, to a previously found optimal R_A , that maintains the set C consistent. Namely, it maximizes the number of differences between the reactions contained in P_A and P_{A^*} . OP₄ inherits constraints 1-9 from OP₃, and incorporates three new constraints. Constraint 10 guarantees that the cardinality of P_{A^*} equals that of the previous optimal P_A in OP₃. Constraint 11 introduces two additional binary variables, δ^+ , δ^- , which measure the mismatches between the vectors x ,

selecting the reactions in P_{A^*} , and the optimal vector x_{opt} , selecting the reactions in P_A and previously found by OP₃. Finally, constraint 12 is added to impose a δ^+ XOR δ^- relationship to avoid the trivial optimal solution in which $\delta^+ = \delta^-$,

$$\begin{aligned}
 & \text{max} \quad \|\delta^+ + \delta^-\|_1 \\
 & v = [v_{irr}, v_{for}, v_{back}] \in \begin{matrix} \mathbb{R}^{r^+} \\ 0 \end{matrix}, \\
 & x = [x_{irr}; x_{rev}], \delta^+, \delta^- \in \{0, 1\}^p \\
 & y \in \{0, 1\}^{r^{ext}} \\
 & s.t. \\
 & 1 - 9. \text{ (OP}_3\text{)} \\
 & 10. \|x\|_1 = Z \quad \quad \quad \text{(OP}_4\text{).} \\
 & 11. x + \delta^+ - \delta^- = x_{opt} \\
 & 12. \delta^+ + \delta^- \leq 1
 \end{aligned}$$

However, besides CorEx, OP₄ can be used to generate alternative optimal networks to other network-centered approaches. We just need to set x_{opt} , in constraint 11, to be the optimal x vector of the particular approach under study; in addition, we need to update Z , in constraint 10, to the corresponding number of non-core reactions added by this approach (*i.e.*, the size of P_A). Note that x_{opt} can be easily constructed from the set P_A , which is derived from a particular context-specific model. In addition, a similar constraint to constraint 10 of OP₄, namely $\|x\|_1 \geq Z_{lb}$, may be included in OP₃, as a lower bound to its objective function, where $Z^* \leq Z_{lb} \leq R$, and Z^* is the unconstrained optimum of OP₃. It is in this manner that CorEx allows relaxing the parsimony condition, as commented before, although in this study we did not constrain the CorEx optimum.

Noteworthy, the main advantage of using OP₄ to obtain alternative optimal networks lies in its MILP formulation. This is because, with the exception of CorEx, which also relies on a single MILP, all existing network-centered approaches require iteratively solving a convex optimization problem. For instance, the linear programs behind the consistency testing step of FastCORE (19), or the ones behind the flux balance analysis, iterated over each reaction of the GEM, in CORDA (20). Alternative optima may arise in each one of these iterations, thus exploring the alternative optima space in each case would require an extensive computational effort. In contrast, we circumvent this problem with OP₄ by analyzing the alternative solutions of a single MILP. However, OP₄ only generates a single, maximally different, alternative optimal network. To generate a sample of alternative networks, here we applied OP₄ in an iterative way. We first used OP₄ to obtain a maximally different network to a given optimal context-specific network, and then repeated this process of feeding OP₄ with the successively generated alternative networks until no additional one was found. At that point, we randomly perturbed the last network by changing the state (active or inactive) of 1% of the reactions, and repeated this process until no additional network was found (an implementation of the procedure is provided in S1File). We note that with this iterative process, which we term the AltNet procedure, we do not guarantee an exhaustive enumeration of all maximally different alternative networks. However, as shown in the next section, it sufficed to illustrate the variety found across optimal context-specific extracted networks in this study.

Finally, we use the AltNet procedure to analyze the alternative optima space of CorEx, FastCORE and CORDA. In the latter case, however, OP₄ had to be slightly modified. This is

because CORDA divides the reactions in the GEM into four categories, in contrast to CorEx and FastCORE, where only the core, C , and the non-core set, P , are considered. Concretely, reactions are separated into three groups based on experimental evidence: reactions with *high* (HC), *medium*, (MC) and *negative* (NC) confidence, and an additional group collecting the remaining reactions (OT) in the GEM, for which experimental evidence is not available. In this case, the group HC corresponds to the core set of reactions (*i.e.*, all reactions in HC must be included in the final model), and the other three groups constitute the non-core set P , although reactions in MC are preferentially added over NC and OT reactions. To account for the different reaction groups, we partitioned the vector x in OP_4 into the sets of MC, NC and OT reactions, and evaluated constraint 10 for each of the three sets. In this manner, we guaranteed that an alternative optimal network contained, besides all HC reactions, the same number of MC, NC and OT reactions than the original CORDA optimum.

Alternative optimal solutions in iMAT

As mentioned above, there already exists a procedure to investigate the alternative optima space for iMAT (16). Hence, we considered relevant to apply iMAT to the same context-specific reconstructions examples used in CorEx, and analyze its alternative optimal solutions. Here, we briefly summarize the iMAT method as well as the procedure proposed by the authors to analyze its alternative optima. In addition, we present our novel complementary approach to sample the alternative optima space of iMAT. iMAT aims at maximizing the global similarity between a given expression data set and a feasible flux distribution of the GEM where data is being integrated. Therefore, in this sense, it follows an approach similar to RegrEx. However, iMAT does not directly minimize the distance between data and flux values. Instead, iMAT first integrates experimental information by classifying reactions in the GEM into two groups: one, R_H , populated by reactions with *highly* expressed associated genes (*i.e.*, above a fixed threshold value, ϵ) and another, R_L , by reactions with *lowly* expressed associated genes (*i.e.*, below ϵ). The MILP presented in OP_5 is then solved to maximize the number of active reactions in R_H (with non-zero flux) and the number of inactive reactions in R_L (with zero flux value), subject to the usual mass balance and thermodynamic constraints. This is implemented by maximizing the norm of two vectors of binary variables, y^+ , y^- , that select reactions in R_H to be active and reactions in R_L to be inactive (the extra variable, y^- , is added to account for reversible reactions).

$$\begin{aligned}
 Z_{opt} = \max_{\substack{v \in \mathbb{R}^m \\ y^+, y^- \in \{0,1\}}} & \sum_{i \in R_H} (y_i^+ + y_i^-) + \sum_{i \in R_L} y_i^+ \\
 s.t. & \\
 1. & Sv = 0 \\
 2. & v_{min} \leq v \leq v_{max} \\
 3. & v_i + y_i^+ (v_{min,i} - \epsilon) \geq v_{min,i}, i \in R_H \\
 4. & v_i + y_i^- (v_{max,i} + \epsilon) \leq v_{max,i}, i \in R_H \\
 5. & v_{min,i} (1 - y_i^+) \leq v_i \leq v_{max,i} (1 - y_i^+), i \in R_L
 \end{aligned}
 \tag{OP_5}$$

To deal with alternative optimal flux distributions, authors proposed the following approach (16). First, OP_5 is solved twice for each reaction in the GEM; the first time, the reaction is forced to be active, in the second, to be inactive. The two objective values, $Z_{act(i)}$, $Z_{inac(i)}$, corresponding to the optimizations where reaction i was active and inactive, respectively, are then compared. If $Z_{act(i)} > Z_{inac(i)}$, reaction i is considered to be active (with confidence $Z_{act(i)} - Z_{inac(i)}$), if $Z_{act(i)} < Z_{inac(i)}$, is considered to be inactive (with confidence $Z_{act(i)} - Z_{inac(i)}$) and if $Z_{act(i)} = Z_{inac(i)}$ is taken as undetermined under the data set been integrated. Therefore, with this procedure one can determine the sets of reactions that individually increase the global similarity to data when active and inactive, respectively, and the set of reactions that do not affect the optimum global similarity to data under whatever state, active or inactive. However, it does not provide information about how the states of reactions distribute across the alternative optima space of iMAT. For instance, a given reaction could be classified as active with this procedure and still be either active or inactive across the space of all alternative optimal flux distributions generated by iMAT.

We emphasize that the results obtained through this method do not align qualitatively to the ones obtained for RegrEx and CorEx (by extension FastCORE and CORDA), and hence they have to be interpreted on their own. To make a fair comparison, we propose another procedure to evaluate the alternative optimal space of iMAT (iMAT_{AOS}), which follows a similar approach to the one employed by RegrEx_{AOS}: we first generate a random flux distribution, v_{rand} , and then search for the closest feasible flux distribution, v , that renders the same optimal result, Z_{opt} , found by iMAT. iMAT_{AOS} optimizes the mixed integer quadratic program:

$$\begin{aligned}
& \min_{v, \delta \in \mathbb{R}^m} \quad \frac{1}{2} \|\delta\|_2^2 \\
& y^+, y^- \in \{0, 1\} \\
& s.t. \\
& 1 - 5 \quad (OP_5) \qquad \qquad \qquad (OP_6). \\
& 6. \quad v = v_{rand} + \delta \\
& 7. \quad \sum_{i \in R_H} (y_i^+ + y_i^-) + \sum_{i \in R_L} y_i^+ = Z_{opt}
\end{aligned}$$

OP_6 inherits constraints 1-5 from OP_5 and includes constraint 6, which defines the distance, $\delta = v - v_{rand}$ to be minimized, and constraint 7, which guarantees that v remains within the alternative optimal space of the previous iMAT optimization.

Evaluation of alternative optima from context-specific data integration approaches: Case studies

Here, we illustrate the ambiguity found during the extraction of context-specific flux distributions and metabolic networks. To this end, we apply the methods described in the previous section to two case studies: a leaf-specific scenario, the model plant *Arabidopsis thaliana*, and a human, liver-specific reconstruction. In the first case, we used the AraCORE model, which includes the primary metabolism of *Arabidopsis thaliana* (23), and a leaf-specific gene expression data set, obtained from (24) (Methods). In the second case, we employed Recon1, a well-established human metabolic model (25). Moreover, we considered two different core sets of reactions that were identified as liver-specific by experimental evidence

(taken from [19] and [20]), and upon which the liver reconstructions were built. In addition, we reduced the original metabolic models by taking only the consistent part of them. The resulting models are termed here ReconIred and AraCOREred (see Methods for details).

We first analyzed the alternative optima of $\text{RegrEx}_{\text{LAD}}$, as a representative of flux-centered approaches, in the leaf-specific scenario. Additionally, we evaluated the effect exerted by the ℓ_1 -regularization of $\text{RegrEx}_{\text{LAD}}$ in reducing the volume of the alternative optima space. We then applied CorEx, a network-centered representative, to extract and analyze the alternative optima for the leaf- and the liver-specific reconstructions, and compare its performance with that of FastCORE [19], a well-established approach. In addition, we evaluated the alternative optimal liver-specific networks generated by CORDA, a recently published approach [20]. Finally, we also investigated the alternative optima of iMAT to the leaf- and liver-specific scenario with both, the original approach proposed in [16] and our own complementary method.

Alternative $\text{RegrEx}_{\text{LAD}}$ optima during leaf-specific data integration

After applying $\text{RegrEx}_{\text{LAD}}$ with $\lambda = 0$, we obtained an optimal, leaf-specific flux distribution. We then applied $\text{RegrEx}_{\text{AOS}}$ to evaluate the alternative optima space of the previously obtained optimum. The results from this evaluation confirmed the existence of an alternative optima space for $\text{RegrEx}_{\text{LAD}}$. However, the variability of the flux values at the optimal objective value was not uniform across different reactions. As expected, data-orphan reactions exhibited more broadly distributed flux values at the alternative optima than data-bounded reactions. We quantified this property by the Shannon entropy (Methods), as a measure of uncertainty associated to a data integration problem. In this sense, data-orphan reactions showed a larger mean entropy value of 1.64 in comparison to the value of 0.95 found for the data-bounded reactions (two-sided ranksum test, $p\text{-value} = 1.95 \times 10^{-5}$). However, we found reactions with particularly low or high entropy values in both sets, data-bounded and data-orphan.

This last observation suggests that reactions with low entropy values may be of special importance under the leaf-specific metabolic state. On the other side, high entropy values suggest that the corresponding reactions could operate more freely in the leaf context. For instance, we found that the majority of transport reactions showed large entropy values, in accord with the fact that most transport reactions are data-orphan. Nevertheless, there were some transport reactions with particularly low entropy values, such as: the *TP/Pi translocator* (reaction index 327 in AraCOREred, $H = 0.07$) interchanging glyceraldehyde 3-phosphate and orthophosphate between the chloroplast and cytoplasm, the *P5C exporter* (index 363, $H = 0.01$) exporting 1-Pyrroline-5-carboxylate from mitochondria to cytoplasm and the *ADP/ATP carrier* (index 320, $H = 0.01$), interchanging ATP and ADP also between mitochondria and cytoplasm (for a comparison, the highest entropy value in the rank is $H = 2.92$, corresponding to the *Proline uniporter*, see the complete list in S1 Table). Therefore, the leaf data integration constrains these transport reactions to take a small range of different flux values due to the network context in which they operate, since they are not directly bounded by experimental data. This observation is contrasted by the high entropy values that these same three reactions when no experimental data are integrated, *i.e.*, when a similar sampling procedure is performed in which only mass balance and thermodynamic constraints are imposed (Methods). In this case, all three entropy values are markedly larger ($H > 2$, S1 Table).

We next focused on the entropy values of reversible reactions in the AraCOREred model. Reversible reactions in a GEM usually correspond to reactions for which no thermodynamic

information is available (leaving aside the set which is known to operate close to equilibrium). Therefore, it would be informative to evaluate whether integrating context-specific experimental data in a GEM could be used to fix the direction of such reactions. Interestingly, we found that a large proportion (75.81%) of the reversible reactions carrying a non-zero flux (including data-orphan) had a fixed direction, either forward or backward, in the alternative optima (Table 1). This finding indicates that, even though there is variation in the flux value of reversible reactions, integration of expression data can determine their direction in a given context. Therefore, the proposed approach and findings provide valuable information on how metabolism could be operating under the particular condition.

Table 1. Summary of the alternative optima space of RegrEx_{LAD}.

	$\lambda = 0$	$\lambda = 0.1$	$\lambda = 0.3$	$\lambda = 0.5$
H_{Data}	73.17	71.34	81.77	65.46
H_{Orphan}	86.82	62.18	59.97	36.50
H_{Total}	159.99	133.52	141.74	101.95
\bar{H}_{Total}	1.23	1.03	1.09	0.78
Fixed_{Rev}(%)	75.81	75.81	80.95	98.18
\bar{M}_R (CV)	6.11 (0.35)	7.59 (0.40)	9.58 (0.43)	14.38 (0.41)

For the analyzed sequence of increasing λ -values, it includes: The sum of entropy values for the subset of data-bounded, H_{Data} , and data-orphan, H_{Orphan} , reactions, as well as for all reactions, H_{Total} , the mean entropy value across all reactions, \bar{H}_{Total} , the proportion of reversible reactions with fixed direction in the alternative optima sample, $Fixed_{Rev}$, and the mean number of reaction mismatches (*i.e.*, the Hamming distance), \bar{M}_R (CV stands for coefficient of variation).

Finally, we analyzed the alternative optimal metabolic networks extracted by RegrEx_{LAD}, since the original RegrEx was developed to provide both, a context-specific flux distribution and a metabolic network. In RegrEx, the context-specific (sub)networks are obtained by considering only reactions, together with the associated metabolites, in the GEM that are predicted to be active in the optimal flux distribution (*i.e.*, with absolute flux greater than some small threshold value). Here we focus on the set of active reactions across the sample of alternative optima. Since we focus on the state of a reaction rather than on its alternative optimal flux values, the overall uncertainty of a RegrEx_{LAD} data integration problem should be reduced. From this perspective, we found that the alternative leaf-specific networks shared a large proportion of the reactions. Specifically, a core of 87 reactions was present in all networks, which consisted of, on average, 105.8 reactions (S2 Table). In addition, any pair of alternative networks differed, on average, in ≈ 6 reactions (Table 1).

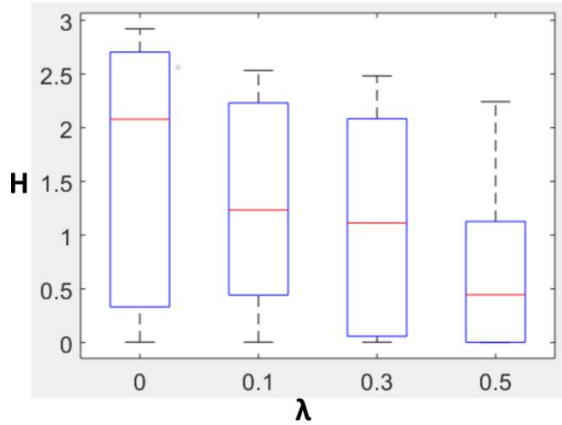
Effect of regularization on the alternative optima space

We next evaluated the RegrEx_{LAD} alternative optima space for a sequence of increasing λ -values. This was motivated to test whether the inclusion of ℓ_1 -regularization, besides imposing sparsity in optimal flux distributions, could also reduce the variability found in individual reaction flux values across the alternative optima space. This property could serve as a way to

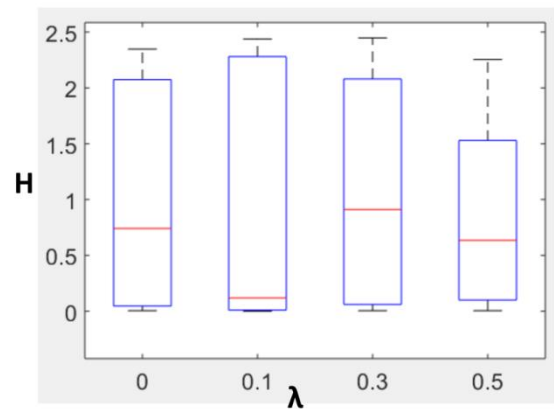
decrease the uncertainty, as measured by the Shannon entropy, associated to a context-specific data integration problem. To this end, we first applied $\text{RegrEx}_{\text{LAD}}$ on AraCOREd and the same leaf data set, but using three increasing λ -values ($\lambda_1 = 0.1$, $\lambda_2 = 0.3$ and $\lambda_3 = 0.5$). We then applied $\text{RegrEx}_{\text{AOS}}$ to sample the alternative optima space of each of the three $\text{RegrEx}_{\text{LAD}}$ data integrations.

We found that the entropy tended to decrease with increasing λ -values, although the effect was more pronounced for the data-orphan reactions (Table 1, Fig 3). For instance, the sum of entropy values among data-orphan reactions decreased from a value of $H_{\text{Orphan}} = 86.82$ for $\lambda = 0$, to $H_{\text{Orphan}} = 36.50$ with $\lambda = 0.5$. In contrast, for the data-bounded reactions, it only decreased from a value of 73.17 with $\lambda = 0$ to 65.46 with $\lambda = 0.5$, and even led to a transient increase at $\lambda = 0.3$ (Table 1, Fig 3). These findings suggest that the inclusion of regularization can reduce the uncertainty associated to a context-specific data integration problem. Naturally, there is a trade-off between decreasing uncertainty and increasing sparsity of the obtained models, since greater λ -values also produce smaller models that may exclude reactions that are relevant to a particular context (SFigure1). However, a mild regularization ($\lambda = 0.1$) already had a substantial effect in reducing the uncertainty of the $\text{RegrEx}_{\text{LAD}}$ data integration in this analysis. Specifically, it decreased the total model entropy, defined as the sum of entropy values over all reactions, by 16.54% (from a value of $H_{\text{Total}} = 159.99$ for $\lambda = 0$, to $H_{\text{Total}} = 133.52$ with $\lambda = 0.1$, Table 1).

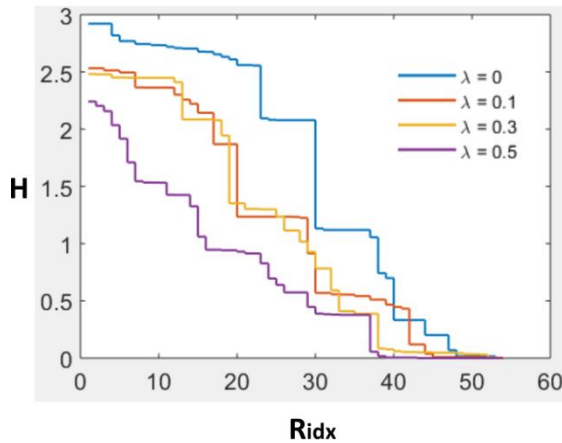
(A) Data-orphan



(B) Data-bounded



(C) Data-orphan



(D) Data-bounded

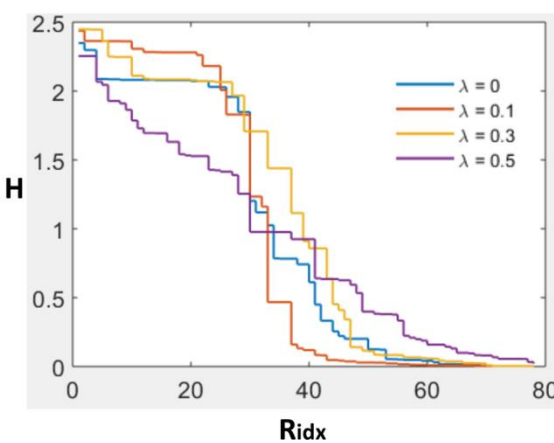


Fig 3. Effect of regularization on the alternative optima space of ReGrEx_{LAD}. The distribution of Shannon entropy values, H , is depicted as box plots for all data-orphan (A) and data-bounded (B) reactions in AraCOREd, across increasing λ -values. Median values, represented by red lines, decrease monotonically only in data-orphan reactions (bottom and upper edges in the box plots indicate the 25th and 75th percentile, respectively). Individual entropies for each data-orphan (C) and data-bounded (D) reaction are also presented in decreasing order for the four λ -values (reactions with $H < 10^{-3}$ are omitted). In data-orphan reactions, all distributions with $\lambda > 0$ fall below the corresponding to $\lambda = 0$ (without regularization, depicted in blue), which is not the case in data-bounded reactions.

Finally, we focused on the effect that regularization had on reversible reactions. We found that the number of reversible reactions with fixed direction increased monotonically with increasing λ -values (Table 1). Hence, this finding suggests that a mild regularization can further constrain the direction in which a reversible reaction can proceed under a particular metabolic context.

Alternative optima in leaf- and liver-specific metabolic networks

We first applied CorEx and FastCORE to reconstruct two leaf-specific networks, Leaf_{CorEx} and Leaf_{FastCORE}. To this end, we used the AraCOREd model and a core set of 91 reactions, which was previously obtained by considering reactions for which the associated gene expression data had a value greater than the 70th percentile (Methods). Both Leaf_{CorEx} and Leaf_{FastCORE}, contained the core set and were consistent, *i.e.*, all reactions were unblocked. However, we noticed that Leaf_{CorEx} was more compact than Leaf_{FastCORE}, containing 236 versus 254 non-core reactions, respectively (Table 2). We next reconstructed the two liver-specific networks in a similar way. To this end, we used the Recon1red model, and the core set of 1069 reactions defined in the original FastCORE publication (19). In this case, CorEx added 593 non-core reactions to the core set, obtaining the liver-specific reconstruction Liver_{CorEx}. FastCORE, on the other hand, added 677 non-core reactions to generate Liver_{FastCORE}. Hence, CorEx was able to extract a more compact liver-specific network, resembling the behavior found in the leaf-specific case. After obtaining these context-specific metabolic reconstructions, we searched for alternative optimal networks to all of them, using the AlterNet procedure describe in the previous section. To quantify the uncertainty of the leaf- and liver-specific reconstructions, we looked at the number of reaction mismatches between all pairs of alternative networks in each case (computed as the Hamming distance, see Methods).

Table 2. Summary of the alternative optima space of CorEx.

	P	#models	M_{Rmax}	$\overline{M_R}$ (CV)	p-value
Leaf_{CorEx}	236	61	52	29.03(0.29)	0
Leaf_{FastCORE}	254	201	118	66.76(0.54)	
Liver_{CorEx}	593	4	156	108.33(0.37)	0.0022
Liver_{FastCORE}	677	100	398	247.93(0.46)	
Liver_{CORDA}	1527	104	992	545.22(0.42)	0
Liver_{CORDAtest}	1527	18	860	389.40(0.48)	

This table summarizes the results of the evaluation of the CorEx alternative optima space. It includes the number of added non-core reactions, P , the maximum, M_{Rmax} , and the mean number, $\overline{M_R}$ (CV stands for coefficient of variation), of reaction mismatches (*i.e.*, Hamming distance) across the alternative networks

for the leaf- and the liver-specific scenarios evaluated by two methods, CorEx and FastCORE. The last column displays the p-value resulted from a two-sided ranksum test comparing the distributions of Hamming distances between any pair of the alternative networks of CorEx and FastCORE (the null hypothesis states that the distribution generated by CorEx is bigger than that of FastCORE).

We found marked differences between alternative optimal networks in both approaches and metabolic scenarios. In the case of Leaf_{CorEx}, 29 non-core reactions differed on average between alternative networks, with a maximum value of 52 reactions (22% of the added non-core reactions). While, in Leaf_{FastCORE}, networks differed on average in 66.78 reactions, and had a maximum number of 118 discrepant reactions (46.5%, Table 2). This situation was even worsened in the liver-specific reconstructions. Between alternative networks to Liver_{CorEx}, we found a maximum of 156 discrepant reactions among the 593 in the added non-core (26.3%), with an average of 108.3. In the case of Liver_{FastCORE}, the maximum number of discrepant reactions was as high as 398 out of the 677 (58.8%) added non-core reactions, with an average of 246.93 between alternative optimal networks (Table 2).

As a complementary analysis, we also determined the frequency of occurrence of every non-core reaction across the alternative optimal networks. In this manner, we could identify: (i) a set of non-core reactions that were always included, termed the active non-core set, (ii) a set of non-core reactions that were excluded from all alternative networks, termed the inactive non-core set, and (iii) a set of non-core reactions that were included in some of the networks, referred to as the variable non-core set. In this case, we took the size of the variable non-core set as a measurement of the uncertainty of a context-specific network extraction; 28% and a 47% of the total non-core reactions were in the variable set in the cases of Leaf_{CorEx} and Leaf_{FastCORE}. On the other hand, a 12% and a 58% were found in Liver_{CorEx} and Liver_{FastCORE}, respectively (Fig 4, A-D).

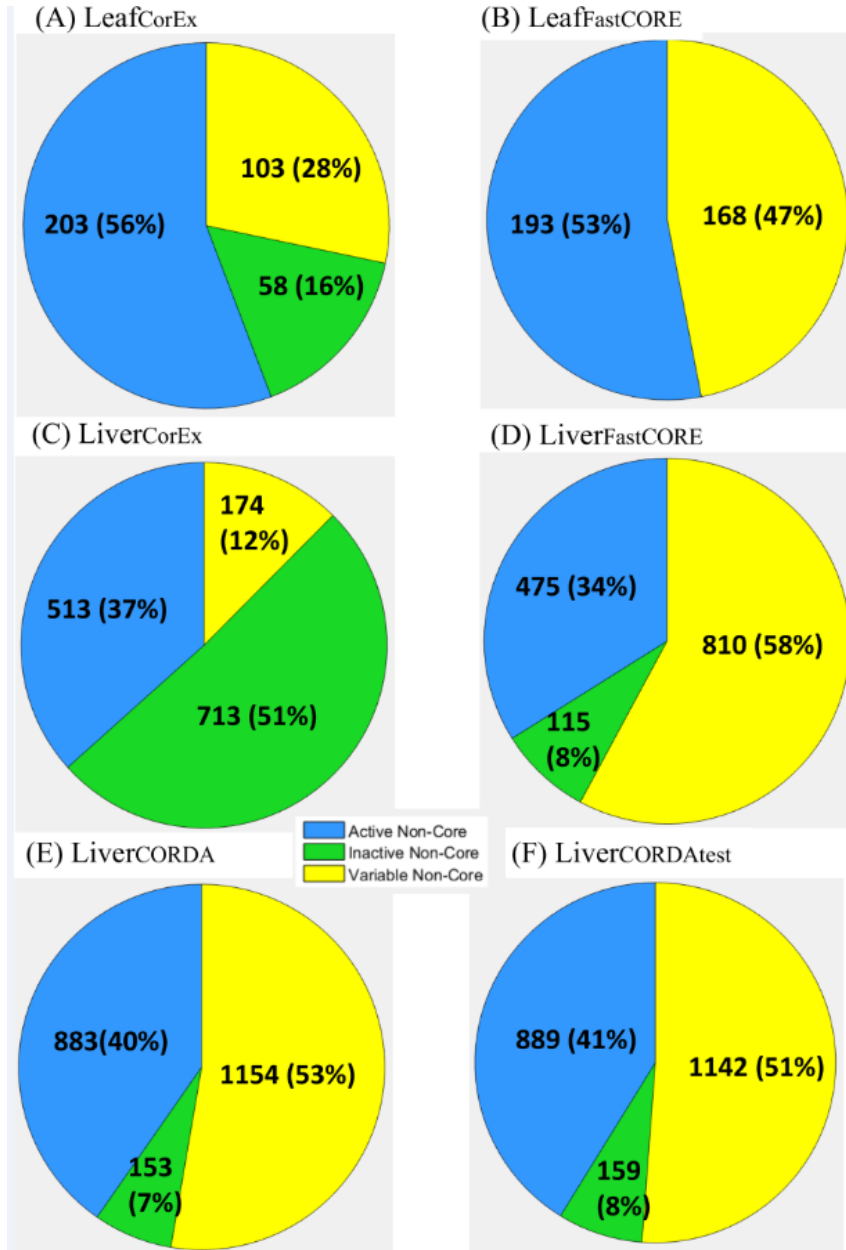


Fig 4. Alternative optima of CorEx and FastCORE context-specific network extractions. The results are divided into the leaf-specific scenario for the CorEx (A) and FastCORE (B) alternative optima, and the liver-specific scenario, for CorEx (C) and FastCORE (D). In all cases, non-core reactions are partitioned into the set that is always included in all alternative networks, (the fixed non-core set, in green), the set that is always excluded (excluded non-core, grey) and the variable non-core set (yellow) which is formed by reactions that are included in some of the alternative networks. In both, the leaf- and the liver-specific scenario, the alternative optima networks generated by CorEx contain a larger proportion of fixed non-core reactions and a smaller proportion of variable non-core reactions. These differences in behavior may be explained by the greater number of non-core reactions that are added by FastCORE, as compare to CorEx, in the optimal solution (see main text).

Finally, we analyzed the alternative optima space of CORDA, a recently published network-centered approach (20). As explained in the previous section (Computational methods) CORDA differs to CorEx and FastCORE in two ways. On one hand, CORDA does not aim at obtaining compact or parsimonious models, but rather emphasizes the metabolic functionality of the final context-specific reconstructions. On the other hand, CORDA considers four groups of reactions

based on experimental evidence, out of which only one, the high confidence core set (HC), has to be fully included in the final model (thus being equivalent to the core set of CorEx and FastCORE). In this case, a suitable alternative optimal network must contain not only the entirety of the HC set, but exactly the same number of reactions added by CORDA in each one of the three remaining groups: the medium (MC) and the negative confidence (NC) groups, and the reactions without experimental data (OT). Therefore, it is reasonable to expect that this additional constraint may reduce the uncertainty of the CORDA reconstructions. To test this idea, we searched for alternative networks to the CORDA liver reconstruction (here $\text{Liver}_{\text{CORDA}}$) provided in (20). $\text{Liver}_{\text{CORDA}}$ was obtained from Recon1 and experimental evidence from the Human Protein Atlas (13), and contains 279 HC, 369 MC, 11 NC and 1147 OT reactions. We used again our AltNet procedure, Recon1red (since blocked reactions, by definition, can never be included in a final network), and the classification of the reactions in the four groups also provided in (20). We were indeed able to find alternative networks to the original $\text{Liver}_{\text{CORDA}}$ with marked differences among them. Concretely, a maximum number of 992 discrepant reactions between two alternative networks, out of the total 1527 distributed among the MC, NC and OT groups (65%, Table 2), with a mean number of 545.22. Similarly, 51% of the non-core reactions (MC, NC and OT) in Recon1red were assigned to the variable non-core set (Fig 4, E).

The examples presented here show that the context-specific reconstructions are more ambiguous than specific, especially in the human liver scenario. This latter case is of special concern, given the implications of obtaining accurate context-specific reconstructions in biomedical research. In fact, most, if not all, of the network-centered approaches have focused on human metabolism (19–22). There are ways, however, to cope with this ambiguity or uncertainty of context-specific reconstructions. For instance, as commented before, CORDA aims at obtaining functional reconstructions. In fact, the authors in (20) tested the capability of the $\text{Liver}_{\text{CORDA}}$ model to conduct a basic set of liver metabolic functions, including aminoacid, sugar and nucleotide metabolism.

We evaluated the alternative $\text{Liver}_{\text{CORDA}}$ models with the same test (Methods), and extracted the subset that passed it. Among these networks, we found that the number of discrepancies and the size of the variable non-core were significantly reduced, as compared to the total set of alternative networks (Table 2, Fig 4, E-F). This is not surprising, since requiring the alternative networks to fulfill certain metabolic functions indirectly imposes an additional constraint to the optimal solution. On the other hand, this additional constraint can also be realized by augmenting the core set, as to guarantee that certain key reactions are present in the final context-specific network. This relates to an additional way to reduce the ambiguity of the reconstruction. In the case studies evaluated here, we found that the CorEx alternative networks tended to be more similar among each other than that of FastCORE or CORDA, as quantified by the (normalized by non-core size) number of discrepancies (Table 2). These differences may be explained by the number of non-core reactions included in the optimum: CorEx obtained more compact models than FastCORE in the Leaf- and the Liver-specific case. This imposes a more stringent constraint when searching for alternative optimal networks. However, there is a tradeoff between model parsimony and functionality. In fact, the $\text{Liver}_{\text{CorEx}}$ model was not able to pass the metabolic function test, while $\text{Liver}_{\text{FastCORE}}$ was able to pass it. In this particular case, $\text{Liver}_{\text{CorEx}}$ did not contain the 9 basal exchange reactions (Methods) required to perform the metabolic functions in the test. However, including these 9 reactions in the liver core set sufficed to generate a $\text{Liver}_{\text{CorEx}}$ model that passed the test..

Finally, the analysis of the alternative optima space can be employed to cope with the ambiguity of a context-specific network reconstruction. Ranking the non-core reactions by their frequency of occurrence among the alternative networks allows to weight reactions by their importance in a given context. Non-core reactions that occur with high frequency in alternative optima should be preferentially included in the final network, while reactions with a low frequency should be discarded. To guarantee that the final network is consistent (*i.e.* the core set is active) one could either (i) add reactions in decreasing order of frequency until consistency is reached, or (ii) select the alternative optimal network that contains the maximum number of highly frequent reactions. Naturally, this approach requires the development of competent methods to sample the alternative space of network-centered approaches. In this sense, we consider our proposed AltNet procedure a first step.

Alternative optimal solutions in the iMAT method

We next applied iMAT and the procedure to analyze its alternative optimal solutions, which we call here iMAT_{FVA} (Methods), to AraCOREd and Recon1red. In this case, we used the core set of reactions for the leaf and the liver contexts as the R_H group in iMAT. In this way, we obtained a leaf-specific model containing 131 reactions and 154 metabolites, while the liver-specific model consisted of 1235 reactions and 1067 metabolites. By applying iMAT_{FVA}, we found a total of 272 active, 178 inactive and 5 undetermined reactions across the iMAT alternative optima space for the leaf context. For the liver context, the alternative optima space included 1223 active, 981 inactive and 143 undetermined reactions in the case of liver (Table 3). We quantified the uncertainty of the iMAT data integration problem by taking the proportion of undetermined reactions over the total number in the GEM. The undetermined reactions in the alternative optima space for the leaf and the liver- contexts were 1.1% and 6.1%, respectively.

Table 3. Summary of the alternative optima space of iMAT.

	Leaf				Liver			
	A	I	U	\overline{M}_R (CV)	A	I	U	\overline{M}_R (CV)
iMAT _{FVA}	272	178	5	-	1223	981	143	-
iMAT _{AOS}	275	40	140	43.16(0.20)	1069	247	1153	369.32(0.05)
Overlap	259 (95.2%)	35 (19.7%)	0	-	928 (75.9%)	69 (5.6%)	2 (0.16%)	-

This table includes the number of active, A, inactive, I, and undetermined, U, reactions across the alternative optima space as determined by iMAT_{FVA} and the iMAT_{AOS}. The intersection between the two methods is also displayed for each of the three categories (Overlap). Finally, the mean number of reaction mismatches (*i.e.*, the Hamming distance), \overline{M}_R , between the generated alternative optimal networks (see main text) is also displayed (the coefficient of variation, CV, is shown in parenthesis). These figures are displayed for the leaf- and the liver-specific scenario.

We next evaluated the alternative optimal space with iMAT_{AOS}, which allowed us to draw two random samples (size $n = 2000$) of leaf- and liver-specific alternative optimal flux distributions. We focused on characterizing the state of the reactions, as active or inactive, across the sample. For the leaf context, 60% of the reactions were active in all alternative flux distributions, 9.23% had a fixed inactive state, and a 30.8% were of undetermined state across the sample. For the liver context, the fraction of fixed active reactions amounted to a 43.3%, 9.52% showed fixed

inactive state, and 47.2% of the reactions were of undetermined state across the sample (Table 3). Here, too, we considered the fraction of reactions with undetermined state across the alternative optima sample as an uncertainty measure of the iMAT data integration problem. Our results demonstrated that the uncertainty for the liver context was greater than that for the leaf (Table 3), which agrees with the results previously obtained in the case of CorEx. These findings were supported by the significantly different Hamming distance calculated between any possible pair of alternative optimal networks (two sided ranksum test, p -value = 0, see Methods). To extract a less ambiguous network, here too, we suggest to rank reactions in the GEM according to their frequency across the alternative optimal iMAT networks (S3 Table contains a complete list of the reaction rankings for leaf and liver). These frequencies can be considered as a measure of the importance that a reaction has under the particular context being evaluated.

Finally, a comparison of the results obtained through the two alternative methods, iMAT_{FVA} and iMAT_{AOS}, showed a good agreement in the sets of reactions classified as active across the alternative optima space: a 94.8% of active reactions per iMAT_{FVA} were also found active by iMAT_{AOS} in the leaf context, and a 75.9 % for the liver context. However, this agreement did not hold in the case of inactive and undetermined reactions, both in leaf and in liver (Table 3). Therefore, this comparison highlighted the importance of analyzing a sample of alternative optimal solutions to obtain a more complete understanding of the uncertainty associated to an experimental data integration problem.

Conclusions

We analyzed the space of alternative optima resulting from the integration of context-specific data into GEMs. To this end, we evaluated a representative from the flux- and network-centered approaches. We selected ReGrEx (18) as a representative of flux-centered approaches and CorEx, as a network-centered approach proposed in this study. In addition, we adapted CorEx to obtain alternative optimal networks for FastCORE (19) and CORDA (20), two state-of-the-art network-centered approaches. Finally, we evaluated the alternative optima of iMAT with the original approach proposed by the authors (16) and another approached designed here. We compared the developed approaches and implemented tools on two illustrative case studies: (i) a medium size GEM of the primary metabolism of *Arabidopsis thaliana* (23) and a leaf-specific gene expression data set (24), and (ii) a larger GEM collecting a reconstruction of a human metabolic network (25) and two liver-specific core sets of reactions (19,20).

Our findings demonstrated the existence of a space of alternative optima for all evaluated approaches integrating context-specific data. Consequently, this space of alternative optima induces ambiguous context-specific reconstructions. In the case of flux-centered approaches, ReGrEx_{LAD} in this study, we proposed the usage of a mild regularization to mediate the uncertainty of the resulting context-specific fluxes. In network-centered approaches, our results showed the existence of markedly disparate alternative context-specific networks in CorEx, FastCORE and CORDA. In addition, a delicate balance between model parsimony and metabolic functionality seems key to reducing the ambiguity of the context-specific reconstructions. An evaluation of the alternative optima space followed by a ranking of the reactions according to their frequency may serve as a way to determine their context-specificity. On this line, we proposed the AltNet procedure to generate alternative optimal context-specific networks. Finally, iMAT_{AOS}, our proposed method to explore the alternative optimal space of iMAT, enabled a more thorough inspection of its alternative optimal space and complements the

results obtained by the method proposed in the original iMAT publication. Our solution allowed ranking reactions according to their likelihood to be active under the evaluated context, which can be taken as a measure of their relative importance in a specific context.

As a concluding remark, we acknowledge the utility of the existent experimental data integration methods, since they allow a fast and automated generation of context-specific flux distributions and metabolic networks. However, our findings indicated that the interpretation and further usage of their results warrant caution. Specially, since the existence of alternative optima is likely linked to the nature of the context-specific data integration problem, and thus is independent of the approach used. The latter claim is supported by our evaluation across qualitatively different approaches. We advocate the view that an analysis of alternative optimal solutions should be performed, whenever possible, if context-specific data are integrated in metabolic models. In the case of context-specific networks reconstructions, more reliable results could be obtained from subsequent careful knowledge-based curation.

Methods

This section contains the details about the implementation of the methods described in this study, the GEMs and context-specific data employed in the case examples, and the computation of the distance metric between alternative optimal networks. In addition to this section, the MATLAB code containing the entire workflow followed in this study can be found in the Supplementary Information.

RegrEX_{LAD}, RegrEX_{AOS}, CorEx and AltNet implementations

All optimization programs used in this study, (*i.e.*, OP₁₋₆) were implemented in MATLAB and solved using Gurobi (version 6.04) (26). All generated code with the implementations is available as Supplementary Information.

Metabolic model and gene expression data

A reduced version of the original AraCORE model (23) was used in this study: AraCORE contains 549 reactions and 407 metabolites assigned to four subcellular compartments, whereas the herein used version (AraCOREred) contains 455 reactions and 374 metabolites. The reactions that were removed correspond to exchange reactions that directly connect organelles to the environment (circumventing the cytoplasm), and were eliminated to avoid bias in the obtained flux distributions. AraCOREred can be found in the Supplementary Material.

Gene expression was taken from (24), stored in the GEO database under the accession numbers GSM852923, GSM852924 and GSM852925 corresponding to *Arabidopsis thaliana* Col-0 lines with no treatment. The corresponding CEL files were normalized using the RMA (Robust Multi-Array Average) method implemented in the *affy* R package (27). In addition, probe names were mapped to gene names following the workflow described in (28), where probes mapping to more than one gene name are eliminated. Gene values were then scaled to the maximum value and mapped to reactions in the AraCOREred model following the included Gene-Protein-Reaction rules and a self-developed MATLAB function, *mapgene2rxn*, which is available in S1File. This process was repeated for the three samples in the dataset and mean values were taken as representative values to obtain the final leaf-specific data used in this study.

We removed blocked reactions from the original Recon1 model to get the Recon1red model used in this study. To this end, we performed a Flux Variability Analysis (see next section) and removed reactions with a maximum absolute flux, $|v_i| < 10^{-6}$. The Flux Variability Analysis was implemented in the MATLAB function *reduceGEM* which also extracted the reduced model, Recon1red, in a COBRA compatible MATLAB structure. The function is available in SFile1.

Extreme flux values of the flux cone

The minimum and maximum allowed values of each reaction in AraCOREred were determined through Flux Variability Analysis (4). Although only the mass balance and the thermodynamic constraints were imposed (*i.e.*, no reaction was forced to take a fraction of a previously calculated optimal value). This was accomplished through the following mathematical program,

$$\begin{aligned} & \min / \max v_i, \quad \forall i \in v \\ & s.t. \\ & S v = 0 \\ & v_{\min} \leq v \leq v_{\max}, \end{aligned}$$

which was implemented in MATLAB and solved with the Gurobi solver (version 6.04). The own-developed MATLAB function can be found in Supplementary Material under the name of *FVA*.

Sampling flux distributions from the flux cone

To evaluate to what extent the Leaf data integration affected the entropy values of the reactions in the AraCOREred model, we also sampled the space of feasible flux distributions (*i.e.*, the flux cone) when no experimental data was been integrated. To this end, and to allow direct comparability of the results, the flux cone was sampled following a similar approach as in RegrEx_{AOS}: first, we generated a random vector of flux values, v_{rand} , within the minimum and maximum values obtained by regular Flux Variability Analysis. The closest flux vector v to v_{rand} within the flux cone was then obtained by minimizing the Euclidean distance between the two vectors. The following quadratic program was used to this end:

$$\begin{aligned} & \min_v \frac{1}{2} \|v - v_{rand}\|_2^2 \\ & s.t. \\ & S v = 0 \\ & v_{\min} \leq v \leq v_{\max}. \end{aligned}$$

This procedure was iterated to obtained a sample of size $n = 2000$. After the sample was generated, we obtained the entropy values of the samples in the same way as when evaluating the alternative optima space of RegrEx_{LAD}. The MATLAB function implementing this sampling procedure can be found in S1File under the name *coneSampling*.

Quantification of the RegrEx_{LAD} alternative optima space

The Shannon entropy of the sampled alternative optima distribution, H_i , was used to quantify the extent to which the flux values of a reaction, i , varied across the alternative optima space. It was calculated as follows:

$$H_i = - \sum_{k=1}^n f_{i,k} \log (f_{i,k}) .$$

Where $f_{i,k}$ represents the frequency (*i.e.*, number of counts relative to sample size) of the k interval in the distribution, for $n = 20$ equally spaced flux value intervals within the flux range of i . In addition, the total entropy of an alternative optima space, H_T , was defined as the sum of the entropies corresponding to the r reactions in AraCOREd, *i.e.*,

$$H_T = \sum_{i=1}^r H_{v(i)} ,$$

and was taken as a measure of the total flux variability found in a particular alternative optima space.

Generation of metabolic networks from context-specific flux distributions and calculation of network distance

In the case of RegrEX_{LAD} and iMAT, we generated the set of alternative optimal metabolic networks from the set of sampled alternative optimal flux distributions. To this end, we first generated the binary vector representations of the flux distributions. The binary vector representations were generated by assigning a value of 1 to the entries corresponding to reactions with a flux value $v \geq 10^{-6}$, and 0 otherwise. This process was repeated for each sampled alternative optimal flux distribution. In addition, repeated vector representations were removed from the generated set. After the binary representations were obtained, we calculated the number of mismatches between any pair, a, b , of binary vectors, with $a \neq b$, *i.e.*, the Hamming distance,

$$M_{R(a,b)} = \sum_{k=1}^n | a_{(i)} - b_{(i)} | .$$

In this way, we obtained a distribution of M_R values whose characteristics were reported and compared.

Implementation of the metabolic test applied to the liver-specific reconstructions

We performed the same metabolic test proposed in (20) and applied to the original Liver-specific CORDA reconstruction. This test consists of a list of metabolic tasks that a metabolic model has to perform, including parts of the aminoacid, sugar and nucleotide metabolism. Concretely, there are a total of 48 metabolic tasks, divided into the production of different aminoacids from minimal metabolic sources and the excretion on urea (19 tasks), the ability to synthesize glucose from 21 different sources (including some aminoacids), and the production of all 5 nucleotides and nucleotide precursors (8 tasks). The details about these tasks can be found in the original CORDA publication (20), while the MATLAB code of our implementation

of this test is provided in S1File. In this study, we used the fraction of performed tasks as measure of the ability of a given liver-specific model to pass this test. For instance, the liver-specific model provided in (20) (under the name of liverCORDAnew), was able to pass 89.58% of the tasks (43 out of 48). In this study, however, we required to pass all tasks in the test to consider an alternative liver-specific network as functional. We realized that, in the liverCORDAnew model, some reactions were slightly different to the analogous reactions in the Recon1red model that we used throughout this study (likely due to different versions of the Recon1 model, which is periodically updated (29)). When we reconstructed our Liver_{CORDA} model, using the same reaction identifiers in liverCORDAnew but extracting the reactions from our Recon1red version, we found that the generated model passed all metabolic 48 tasks in the test. Hence, for consistency of the results, we considered that all proper alternative optimal networks to Liver_{CORDA} had to pass all 48 tasks as well.

iMAT implementation and alternative optima evaluation

The iMAT implementation was taken from the function *createTissueSpecificModel* in the COBRA toolbox (30) (for MATLAB) and slightly modified to allow the usage of the Gurobi solver, used throughout this study. In addition, the iMAT_{FVA} procedure was performed through adapting the previous iMAT implementation (no publicly available implementation of this procedure was found). Both MATLAB functions can be found in S1File under the names of *iMAT* and *iMAT_{FVA}*. In addition, the implementation of our alternative sampling method, *iMAT_{AOS}*, can be found in the same file.

References

1. Lewis NE, Nagarajan H, Palsson BO. Constraining the metabolic genotype–phenotype relationship using a phylogeny of in silico methods. *Nature Reviews Microbiology*. 2012.
2. Bordbar A, Monk JM, King Z a, Palsson BO. Constraint-based models predict metabolic and associated cellular functions. *Nat Rev Genet* [Internet]. 2014;15:107–20. Available from: <http://www.ncbi.nlm.nih.gov/pubmed/24430943>
3. Boyd S, Vandenberghe L. *Convex Optimization* [Internet]. Optimization Methods and Software. 2010. 487–487 p. Available from: https://web.stanford.edu/~boyd/cvxbook/bv_cvxbook.pdf
4. Mahadevan R, Schilling CH. The effects of alternate optimal solutions in constraint-based genome-scale metabolic models. *Metab Eng*. 2003;5(4):264–76.
5. Lee S, Phalakornkule C, Domach MM, Grossmann IE. Recursive MILP model for finding all the alternate optima in LP models for metabolic networks. *Comput Chem Eng* [Internet]. 2000 Jul [cited 2016 Feb 21];24(2-7):711–6. Available from: <http://www.sciencedirect.com/science/article/pii/S0098135400003239>
6. Reed JL, Palsson BØ. Genome-scale in silico models of E. coli have multiple equivalent phenotypic states: assessment of correlated reaction subsets that comprise network states. *Genome Res* [Internet]. 2004 Sep 1 [cited 2016 Feb 21];14(9):1797–805. Available from: <http://genome.cshlp.org/content/14/9/1797.full>
7. Binns M, de Atauri P, Vlysidis A, Cascante M, Theodoropoulos C. Sampling with

- poling-based flux balance analysis: optimal versus sub-optimal flux space analysis of *Actinobacillus succinogenes*. *BMC Bioinformatics* [Internet]. BioMed Central; 2015 Feb 18 [cited 2016 Jan 11];16(1):49. Available from: <http://bmcbioinformatics.biomedcentral.com/articles/10.1186/s12859-015-0476-5>
8. Kelk SM, Olivier BG, Stougie L, Bruggeman FJ. Optimal flux spaces of genome-scale stoichiometric models are determined by a few subnetworks. *Sci Rep* [Internet]. Nature Publishing Group; 2012 Jan 15 [cited 2016 Feb 21];2:580. Available from: <http://www.nature.com/srep/2012/120815/srep00580/full/srep00580.html>
 9. Müller AC, Bockmayr A. Flux modules in metabolic networks. *J Math Biol* [Internet]. 2014 Nov [cited 2016 Feb 26];69(5):1151–79. Available from: <http://www.ncbi.nlm.nih.gov/pubmed/24141488>
 10. Barrett T, Wilhite SE, Ledoux P, Evangelista C, Kim IF, Tomashevsky M, et al. NCBI GEO: archive for functional genomics data sets--update. *Nucleic Acids Res* [Internet]. 2013 Jan [cited 2016 Apr 3];41(Database issue):D991–5. Available from: <http://www.pubmedcentral.nih.gov/articlerender.fcgi?artid=3531084&tool=pmcentrez&rendertype=abstract>
 11. Kopka J, Schauer N, Krueger S, Birkemeyer C, Usadel B, Bergmüller E, et al. GMD@CSB.DB: the Golm Metabolome Database. *Bioinformatics* [Internet]. 2005 Apr 15 [cited 2016 May 26];21(8):1635–8. Available from: <http://www.ncbi.nlm.nih.gov/pubmed/15613389>
 12. Petryszak R, Burdett T, Fiorelli B, Fonseca NA, Gonzalez-Porta M, Hastings E, et al. Expression Atlas update--a database of gene and transcript expression from microarray- and sequencing-based functional genomics experiments. *Nucleic Acids Res* [Internet]. 2014 Jan [cited 2016 May 26];42(Database issue):D926–32. Available from: <http://www.pubmedcentral.nih.gov/articlerender.fcgi?artid=3964963&tool=pmcentrez&rendertype=abstract>
 13. Marx V. Proteomics: An atlas of expression. *Nature* [Internet]. Nature Publishing Group, a division of Macmillan Publishers Limited. All Rights Reserved.; 2014 May 29 [cited 2016 May 26];509(7502):645–9. Available from: <http://dx.doi.org/10.1038/509645a>
 14. Wishart DS, Jewison T, Guo AC, Wilson M, Knox C, Liu Y, et al. HMDB 3.0-The Human Metabolome Database in 2013. *Nucleic Acids Res*. 2013;41(D1).
 15. Uhlen M, Hallström BM, Lindskog C, Mardinoglu A, Ponten F, Nielsen J. Transcriptomics resources of human tissues and organs. *Mol Syst Biol* [Internet]. 2016;12(4):862–862. Available from: <http://msb.embopress.org/content/12/4/862.abstract>
 16. Shlomi T, Cabili MN, Herrgård MJ, Palsson BØ, Ruppin E. Network-based prediction of human tissue-specific metabolism. *Nat Biotechnol*. 2008;26(9):1003–10.
 17. Recht L, Töpfer N, Batushansky A, Sikron N, Gibon Y, Fait A, et al. Metabolite Profiling and Integrative Modeling Reveal Metabolic Constraints for Carbon Partitioning under Nitrogen-Starvation in the Green Alga *Haematococcus pluvialis*. *J Biol Chem*. 2014;289:30387–403.

18. Robaina Estévez S, Nikoloski Z. Context-Specific Metabolic Model Extraction Based on Regularized Least Squares Optimization. *PLoS One* [Internet]. Public Library of Science; 2015 Jan 9 [cited 2015 Jul 11];10(7):e0131875. Available from: <http://journals.plos.org/plosone/article?id=10.1371/journal.pone.0131875>
19. Vlassis N, Pacheco MP, Sauter T. Fast Reconstruction of Compact Context-Specific Metabolic Network Models. *PLoS Comput Biol*. 2014;10(1).
20. Schultz A, Qutub AA. Reconstruction of Tissue-Specific Metabolic Networks Using CORDA. *PLoS Comput Biol* [Internet]. Public Library of Science; 2016 Mar 4 [cited 2016 Mar 7];12(3):e1004808. Available from: <http://journals.plos.org/ploscompbiol/article/authors?id=10.1371%2Fjournal.pcbi.1004808>
21. Jerby L, Shlomi T, Ruppin E. Computational reconstruction of tissue-specific metabolic models: application to human liver metabolism. *Mol Syst Biol*. 2010;6:401.
22. Wang Y, Eddy J a, Price ND. Reconstruction of genome-scale metabolic models for 126 human tissues using mCADRE. *BMC Syst Biol* [Internet]. 2012;6:153. Available from: <http://www.pubmedcentral.nih.gov/articlerender.fcgi?artid=3576361&tool=pmcentrez&rendertype=abstract>
23. Arnold A, Nikoloski Z. Bottom-up Metabolic Reconstruction of Arabidopsis and Its Application to Determining the Metabolic Costs of Enzyme Production. *Plant Physiol* [Internet]. 2014;165:1380–91. Available from: <http://www.ncbi.nlm.nih.gov/pubmed/24808102>
24. Booker F, Burkey K, Morgan P, Fiscus E, Jones A. Minimal influence of G-protein null mutations on ozone-induced changes in gene expression, foliar injury, gas exchange and peroxidase activity in *Arabidopsis thaliana* L. *Plant Cell Environ* [Internet]. 2012 Apr [cited 2015 Sep 9];35(4):668–81. Available from: <http://www.ncbi.nlm.nih.gov/pubmed/21988569>
25. Duarte NC, Becker SA, Jamshidi N, Thiele I, Mo ML, Vo TD, et al. Global reconstruction of the human metabolic network based on genomic and bibliomic data. *Proc Natl Acad Sci U S A*. 2007;104:1777–82.
26. Gurobi Optimization I. Gurobi Optimizer Reference Manual [Internet]. 2014. Available from: <http://www.gurobi.com>
27. Gautier L, Cope L, Bolstad BM, Irizarry RA. affy--analysis of Affymetrix GeneChip data at the probe level. *Bioinformatics* [Internet]. Oxford University Press; 2004 Feb 12 [cited 2016 Jul 3];20(3):307–15. Available from: <http://bioinformatics.oxfordjournals.org/cgi/doi/10.1093/bioinformatics/btg405>
28. Moyano TC, Vidal EA, Contreras-López O, Gutiérrez RA. Constructing simple biological networks for understanding complex high-throughput data in plants. *Methods Mol Biol* [Internet]. 2015 Jan [cited 2015 Sep 29];1284:503–26. Available from: <http://www.ncbi.nlm.nih.gov/pubmed/25757789>
29. King ZA, Lu J, Dräger A, Miller P, Federowicz S, Lerman JA, et al. BiGG Models: A platform for integrating, standardizing and sharing genome-scale models. *Nucleic Acids*

Res [Internet]. 2016 Jan 4 [cited 2016 Jul 3];44(D1):D515–22. Available from: <http://nar.oxfordjournals.org/lookup/doi/10.1093/nar/gkv1049>

30. Hyduke D, Schellenberger J, Que R, Fleming R, Thiele I, Orth J, et al. COBRA Toolbox 2.0. Protocol Exchange. 2011.

Supplementary Information - Captions

S1 Fig. The $\text{RegrEx}_{\text{LAD}}$ solution path through a sequence of increasing λ -values. A sequence of optimal solutions (*i.e.*, flux distributions) to the leaf-specific $\text{RegrEx}_{\text{LAD}}$ integration problem is presented. The sequence begins with $\lambda = 0$ (*i.e.*, no regularization) and ends with $\lambda = 1$, which is the value for which all fluxes are shrunk to 0. Flux distributions get sparser with increasing values for lambda. In addition, the total entropy of the alternative optima tends to decrease with increasing values for lambda. This indicates the existence of a trade-off between sparsity and entropy reduction. In this study, a mild regularization ($\lambda = 0.1$) seems sufficient to substantially reduce the total entropy value while preventing flux distributions to become too sparse (*i.e.*, in which important reactions for a given context may be excluded).

S1 Table. Ranked list of AraCOREd reactions according to their entropy values across the alternative optima space of $\text{RegrEx}_{\text{LAD}}$. In this list, reactions are ranked in descending order according to their entropy values across the alternative optima space of the $\text{RegrEx}_{\text{LAD}}$ leaf-specific data integration. For each reaction in the list, the reaction index in the AraCOREd model, as well as reaction name, the metabolic subsystem to which it is allocated and the reaction mechanism are displayed. As commented in the main text, the entropy values may be taken as a soft measure of the importance that a reaction has in a given context. This is because small entropy values imply that a reaction is constrained to operate under a small range of flux values in the given context. To contrast the entropy values obtained after the leaf-data integration, we also provide the entropy values shown by reactions when no experimental data are integrated, that is, corresponding to a random sample of the flux cone (see Methods).

S2 Table. Ranked list of AraCOREd reactions according to their frequency across the alternative optima space of the alternative networks generated by $\text{RegrEx}_{\text{LAD}}$.

S3 Table. Ranked list of AraCOREd reactions according to their frequency across the sample of alternative optimal networks of iMAT.

S1 Appendix. Detailed description of $\text{RegrEx}_{\text{LAD}}$ and comparison with the original $\text{RegrEx}_{\text{OLS}}$.

S1 File. MATLAB code containing the implementations of all presented methods as well as the workflow followed to generate all results in this study. The GEM models as well as the (mapped to reaction) expression data used are also included.